Three-dimensional FEM Analysis Program of Dynamic Soil-Structure Interaction for Parallel Computer and Solution Verification

N. Onishi
Tokyo University of Science, Japan

SUMMARY:
Technical trend for speed-up of CPUs has been shifted from single-core to multi-core these days. Although the performances have become higher than a few decades before, it is necessary to shorten processing time and get required amount of memory by using processors and memories in a number of computers for solving large-scale simultaneous linear equations, because the degrees of freedom tend to be large in three-dimensional finite element method analysis. In this paper, a parallelization method applied to the dynamic soil-structure response analysis program is outlined, and the effectiveness of the program was verified by the relationship between degrees of freedom and required processing time, and by calculation results. In comparison with theoretical values of damping ratio due to dissipation damping based on elastic wave theory, the damping ratio calculated from amplitude reduction factors of responses are considered generally valid.

Keywords: Parallel computing; Dynamic soil-structure interaction; Domain decomposition method

1. INTRODUCTION

Superstructures are usually designed based on the premise in structural design that the foundation is designed in accordance with the criterion which doesn't allow it damaged when predicted major earthquake hits. However, it hasn't yet clarified how much the degradation of stiffness and bearing capacity of ground and foundation by the external force which exceeds the design load has an influence on the response of superstructure.

To examine how much is the effect of stiffness and strength of ground and foundation on the response of superstructure, I have made a program that can take account of the dynamic interaction between ground and superstructure with spread foundation using three-dimensional finite element method. This program has been parallelized with message passing interface (MPI), which make it possible to be processed on distributed memory parallel computer.

2. CALCULATION METHODS

Parallel computing, in this paper, is for solving large-scale problems in a short time by dividing the analysis object into some processes of a computer cluster; beside, when solving problems using 3D FEM on parallel computers, parallelization only for linear equations solver is not enough. Thus, to increase in speed of calculation and to save the memory space, domain decomposition method (DDM) developed by Soneda, Yagawa and Yoshimura (1991) and compressed sparse row format (CSR) have been applied to the program.

2.1. Kinematic Equation with Three-Dimensional Viscous Boundary

In the kinematic equation of soil-structure analysis, ground acceleration was input and three-

dimensional viscous boundary was applied to the lateral and bottom boundary around analysis domain to reduce the influence on structure by reflected wave. The equation that solves problems of ground and superstructure without dividing them is described as below.

$$[M]\{{}^t\ddot{u}\}+[C]\{{}^t\dot{u}\}+[K]\{{}^tu\}=-[M]\{{}^t\ddot{u}_g\}+[G_{Ltrl}]\{{}^tu^f\}+([C_{Ltrl}]+[G_{CLtrl}])\{{}^t\dot{u}^f\} \tag{2.1}$$

Here $[M]$, $[C]$, and $[K]$ are matrices of mass, damping, and stiffness of ground. $[G_{Ltrl}]$, $[C_{Ltrl}]$, and $[G_{CLtrl}]$ are a boundary stiffness matrix, a viscous boundary matrix, and a boundary damping matrix of lateral free field out of the analysis domain. $\{{}^tu\}$, $\{{}^t\ddot{u}_g\}$, and $\{{}^tu^f\}$ are vectors of response displacement, ground acceleration, and displacement of lateral free field at time t s.

2.2. Incremental Form of the Newmark-beta Method

Kinematic equation Eqn. 2.1 comes down to an incremental form described as below.

$$[\overline{K}]\{{}^{t+\Delta t}_{t}u\}=\{\overline{{}^{t+\Delta t}_{t}p}\} \tag{2.2}$$

Here $[\overline{K}]$ is an effective stiffness matrix, $\{{}^{t+\Delta t}_{t}u\}$ and $\{\overline{{}^{t+\Delta t}_{t}p}\}$ are vectors of incremental displacement and incremental effective nodal force from time t s to $t+\Delta t$ s. With Newmark-beta method associating Eqn. 2.2 with Eqn. 2.1, $[\overline{K}]$ and $\{\overline{{}^{t+\Delta t}_{t}p}\}$ can be described as follows.

$$[\overline{K}]=[K]+\frac{1}{2\beta\Delta t}[C]+\frac{1}{\beta\Delta t^2}[M] \tag{2.3}$$

$$\begin{aligned}\{\overline{{}^{t+\Delta t}_{t}p}\}=&-[M]\{{}^{t+\Delta t}_{t}\ddot{u}_g\}+[M]\left(\frac{1}{\beta\Delta t}\{{}^t\dot{u}\}+\frac{1}{2\beta}\{{}^t\ddot{u}\}\right)+[C]\left(\frac{1}{2\beta}\{{}^t\dot{u}\}+\left(\frac{1}{4\beta}-1\right)\Delta t\{{}^t\ddot{u}\}\right)\\&+[G_{Ltrl}]\{{}^{t+\Delta t}_{t}u^f\}+([C_{Ltrl}]+[G_{CLtrl}])\{{}^{t+\Delta t}_{t}\dot{u}^f\}\end{aligned} \tag{2.4}$$

Where $\beta = 0.25$ in this study, which yields the constant average acceleration method.

2.3. Application of Domain Decomposition Method

To apply domain decomposition method to Eqn. 2.2, all nodes were sorted into structure (suffix *s*) and ground that includes foundation (suffix *g*), then the ground nodes were sorted into internal nodes (suffix *I*) and inter-subdomain boundary nodes (suffix *B*). Furthermore, internal nodes were sorted into *n* subdomains, and inter-subdomain boundary nodes were sorted into nodes of rigid foundation (suffix *R*) and others (suffix *F*). Coefficient matrices were made for each subdomain, and vectors of internal nodes were made for each subdomain. But vectors of boundary nodes were made not only for each subdomain but also as a whole, as shown in Fig. 2.1.

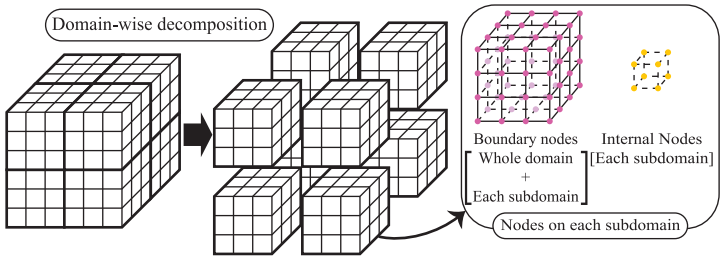

Figure 2.1. Domain-wise decomposition

Then the components of the matrix and the vectors in Eqn. 2.2 can be described as follows.

$$\left[\begin{array}{ccc:c:c} \left[\overline{K_{FF}^g}\right]_{II}^{(1)} & & O & \left[\overline{K_{FF}^g} \quad \overline{K_{FR}^g}\right]_{IB}^{(1)} N_B^{(1)T} & O \\ & \ddots & & \vdots & \vdots \\ O & & \left[\overline{K_{FF}^g}\right]_{II}^{(n)} & \left[\overline{K_{FF}^g} \quad \overline{K_{FR}^g}\right]_{IB}^{(n)} N_B^{(n)T} & O \\ \hdashline N_B^{(1)}\left[\begin{array}{c}\overline{K_{FF}^g}\\ \overline{K_{RF}^g}\end{array}\right]_{BI}^{(1)} & \cdots & N_B^{(n)}\left[\begin{array}{c}\overline{K_{FF}^g}\\ \overline{K_{RF}^g}\end{array}\right]_{BI}^{(n)} & \left[\begin{array}{cc}\overline{K_{FF}^g} & \overline{K_{FR}^g}\\ \overline{K_{RF}^g} & \overline{K_{RR}^g}\end{array}\right]_{BB} & \left[\begin{array}{c}O\\ \overline{K_{Rs}^g}\end{array}\right] \\ \hdashline O & \cdots & O & \left[O \quad \overline{K_{Rs}^g}^T\right] & \overline{K^s} \end{array}\right] \left\{\begin{array}{c} {}_t^{t+\Delta t}u_{FI}^{g\,(1)} \\ \vdots \\ {}_t^{t+\Delta t}u_{FI}^{g\,(n)} \\ \hdashline {}_t^{t+\Delta t}u_{FB}^{g} \\ \hdashline {}_t^{t+\Delta t}\hat{u}_R^{g} \\ \hdashline {}_t^{t+\Delta t}u^{s} \end{array}\right\} = \left\{\begin{array}{c} \overline{{}_t^{t+\Delta t}p_{FI}^{g}}^{(1)} \\ \vdots \\ \overline{{}_t^{t+\Delta t}p_{FI}^{g}}^{(n)} \\ \hdashline {}_t^{t+\Delta t}p_{FB}^{g} \\ \hdashline \overline{{}_t^{t+\Delta t}\hat{p}_R^{g}} \\ \hdashline {}_t^{t+\Delta t}p^{s} \end{array}\right\} \tag{2.5}$$

Here O is a zero matrix and $N_B^{(k)}$ (k=1~n) is a matrix that transforms a force vector of boundary nodes in each subdomain $\{p_B^{(k)}\}$ into that of total boundary nodes in the whole domain $\{p_B\}$. The transpose of $N_B^{(k)}$ is a matrix that transforms a displacement vector of total boundary nodes $\{u_B\}$ into that of boundary nodes in each subdomain $\{u_B^{(k)}\}$. These relationships can be described as follows.

$$\{p_B\} = \sum_{k=1}^{n} N_B^{(k)} \{p_B^{(k)}\} \tag{2.6a}$$

$$\{u_B^{(k)}\} = N_B^{(k)T} \{u_B\} \tag{2.6b}$$

In addition, $\{\hat{p}_R^g\}$ and $\{\hat{u}_R^g\}$ in Eqn. 2.5 are a force vector and a displacement vector of a representative node of rigid foundation, and, with a matrix R for dealing with rigid body, those are associated with a force vector $\{p_R^g\}$ and a displacement vector $\{u_R^g\}$ of ground nodes where rigid foundation is located. Those relationships are described as below.

$$\hat{p}_R^g = R p_R^g, \quad u_R^g = R^T \hat{u}_R^g \tag{2.7a, b}$$

When the rigid foundation has three degrees of freedom (DOFs) shown in Fig. 2.2, the matrix R is given as below.

$$R = \left[R^{(1)} \quad \cdots \quad R^{(i)} \quad \cdots \quad R^{(m)}\right] \text{ where } R^{(i)} = \begin{bmatrix} 1 & 0 & 0 \\ 0 & 0 & 1 \\ -L_z^{(i)} & 0 & L_x^{(i)} \end{bmatrix} \tag{2.8}$$

Here m is a number of ground nodes that consists rigid foundation and $L_x^{(k)}$ and $L_z^{(k)}$ are differences between an original node and the representative node of the foundation in horizontal x-coordinate and vertical z-coordinate, respectively.

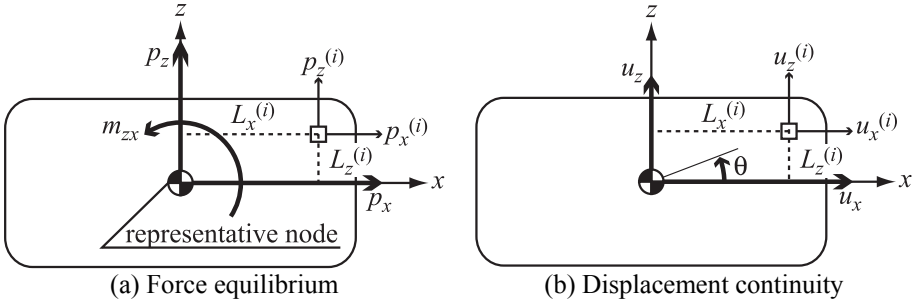

(a) Force equilibrium (b) Displacement continuity

Figure 2.2. Force equilibrium and displacement continuity of rigid foundation

Then Eqn. 2.5 were divided into three equations: internal nodes of each subdomain of ground (Eqn. 2.9), total boundary nodes (Eqn. 2.10), and superstructure (Eqn. 2.11).

$$\left[\overline{K_{FF}^{g}}\right]_{II}^{(k)}\left\{{}_{t+\Delta t}_{t}u_{FI}^{g\,(k)}\right\}+\left[\overline{K_{FF}^{g}}\quad\overline{K_{FR}^{g}}\right]_{IB}^{(k)}N_{B}^{(k)T}\left\{\begin{matrix}{}_{t+\Delta t}_{t}u_{FB}^{g}\\ {}_{t+\Delta t}_{t}\hat{u}_{R}^{g}\end{matrix}\right\}=\left\{{}_{t+\Delta t}_{t}\overline{p_{FI}^{g}}^{(k)}\right\} \tag{2.9}$$

$$\sum_{k=1}^{n}N_{B}^{(k)}\left[\begin{matrix}\overline{K_{FF}^{g}}\\ \overline{K_{RF}^{g}}\end{matrix}\right]_{BI}^{(k)}\left\{{}_{t+\Delta t}_{t}u_{FI}^{g\,(k)}\right\}+\left[\begin{matrix}\overline{K_{FF}^{g}} & \overline{K_{FR}^{g}}\\ \overline{K_{RF}^{g}} & \overline{K_{RR}^{g}}\end{matrix}\right]_{BB}\left\{\begin{matrix}{}_{t+\Delta t}_{t}u_{FB}^{g}\\ {}_{t+\Delta t}_{t}\hat{u}_{R}^{g}\end{matrix}\right\}+\left[\begin{matrix}O\\ K_{Rs}^{g}\end{matrix}\right]\left\{{}_{t+\Delta t}_{t}u^{s}\right\}=\left\{\begin{matrix}{}_{t+\Delta t}_{t}\overline{p_{FB}^{g}}\\ {}_{t+\Delta t}_{t}\hat{p}_{R}^{g}\end{matrix}\right\} \tag{2.10}$$

$$\left[\begin{matrix}O & \overline{K_{Rs}^{g}}^{T}\end{matrix}\right]\left\{\begin{matrix}{}_{t+\Delta t}_{t}u_{FB}^{g}\\ {}_{t+\Delta t}_{t}\hat{u}_{R}^{g}\end{matrix}\right\}+\left[\overline{K^{s}}\right]\left\{{}_{t+\Delta t}_{t}u^{s}\right\}=\left\{{}_{t+\Delta t}_{t}\overline{p^{s}}\right\} \tag{2.11}$$

Solving Eqn. 2.9 for $\left\{{}_{t+\Delta t}_{t}u_{FI}^{g\,(k)}\right\}$ and Eqn. 2.11 for $\left\{{}_{t+\Delta t}_{t}u^{s}\right\}$, the following equations were obtained.

$$\left\{{}_{t+\Delta t}_{t}u_{FI}^{g\,(k)}\right\}=\left[\overline{K_{FF}^{g}}\right]_{II}^{(k)-1}\left(\left\{{}_{t+\Delta t}_{t}\overline{p_{FI}^{g}}^{(k)}\right\}-\left[\overline{K_{FF}^{g}}\quad\overline{K_{FR}^{g}}\right]_{IB}^{(k)}N_{B}^{(k)T}\left\{\begin{matrix}{}_{t+\Delta t}_{t}u_{FB}^{g}\\ {}_{t+\Delta t}_{t}\hat{u}_{R}^{g}\end{matrix}\right\}\right) \tag{2.12}$$

$$\left\{{}_{t+\Delta t}_{t}u^{s}\right\}=\left[\overline{K^{s}}\right]^{-1}\left(\left\{{}_{t+\Delta t}_{t}\overline{p^{s}}\right\}-\left[\begin{matrix}O & \overline{K_{Rs}^{g}}^{T}\end{matrix}\right]\left\{\begin{matrix}{}_{t+\Delta t}_{t}u_{FB}^{g}\\ {}_{t+\Delta t}_{t}\hat{u}_{R}^{g}\end{matrix}\right\}\right) \tag{2.13}$$

Then, substituting Eqn. 2.12 and 2.13 in Eqn. 2.10, Eqn. 2.14 were obtained.

$$\begin{aligned}&\left(\left[\begin{matrix}\overline{K_{FF}^{g}} & \overline{K_{FR}^{g}}\\ \overline{K_{RF}^{g}} & \overline{K_{RR}^{g}}\end{matrix}\right]_{BB}-\sum_{k=1}^{n}N_{B}^{(k)}\left[\begin{matrix}\overline{K_{FF}^{g}}\\ \overline{K_{RF}^{g}}\end{matrix}\right]_{BI}^{(k)}\left[\overline{K_{FF}^{g}}\right]_{II}^{(k)-1}\left[\overline{K_{FF}^{g}}\quad\overline{K_{FR}^{g}}\right]_{IB}^{(k)}N_{B}^{(k)T}\right.\\&\left.-\left[\begin{matrix}O\\ \overline{K_{Rs}^{g}}\end{matrix}\right]\left[\overline{K^{s}}\right]^{-1}\left[\begin{matrix}O & \overline{K_{Rs}^{g}}^{T}\end{matrix}\right]\right)\left\{\begin{matrix}{}_{t+\Delta t}_{t}u_{FB}^{g}\\ {}_{t+\Delta t}_{t}\hat{u}_{R}^{g}\end{matrix}\right\}\\&=\left\{\begin{matrix}{}_{t+\Delta t}_{t}\overline{p_{FB}^{g}}\\ {}_{t+\Delta t}_{t}\hat{p}_{R}^{g}\end{matrix}\right\}-\sum_{k=1}^{n}N_{B}^{(k)}\left[\begin{matrix}\overline{K_{FF}^{g}}\\ \overline{K_{RF}^{g}}\end{matrix}\right]_{BI}^{(k)}\left[\overline{K_{FF}^{g}}\right]_{II}^{(k)-1}\left\{{}_{t+\Delta t}_{t}\overline{p_{FI}^{g}}^{(k)}\right\}-\left[\begin{matrix}O\\ \overline{K_{Rs}^{g}}\end{matrix}\right]\left[\overline{K^{s}}\right]^{-1}\left\{{}_{t+\Delta t}_{t}\overline{p^{s}}\right\}\end{aligned} \tag{2.14}$$

The flow in each time step is shown as follows:

(1) Solve Eqn. 2.14 to get $\left\{{}_{t+\Delta t}_{t}u_{F}^{g}\quad{}_{t+\Delta t}_{t}\hat{u}_{R}^{g}\right\}^{T}$ by conjugated gradient method, then transform it into $\left\{{}_{t+\Delta t}_{t}u_{F}^{g}\quad{}_{t+\Delta t}_{t}u_{R}^{g}\right\}^{T}$ with Eqn. 2.7b.

(2) Solve Eqn. 2.12 and Eqn. 2.13 to get $\left\{{}_{t+\Delta t}_{t}u_{FI}^{g\,(k)}\right\}$ and $\left\{{}_{t+\Delta t}_{t}u^{s}\right\}$, respectively.

(3) Assume response acceleration, velocity, and displacement in the next time step from the incremental displacement obtained above.

(4) Calculate nodal force from displacement.

(5) Calculate unbalanced force $\left\{P^{u}\right\}$ and do convergence test. If it is converged, move on to the next step.

(6) If it is not converged, calculate additional incremental displacement from unbalanced force and renew acceleration, velocity, and displacement. Then back to (4).

The unbalanced force vector $\left\{P^{u}\right\}$ in the flow is given by

$$\begin{aligned}\left\{P^{u}\right\}=&-\left[M\right]\left(\left\{{}_{t+\Delta t}\ddot{u}_{g}\right\}+\left\{{}_{t+\Delta t}\ddot{u}\right\}\right)-\left[C\right]\left\{{}_{t+\Delta t}\dot{u}\right\}-\left[H_{0}\right]\left[R_{0}\right]\left\{{}_{t+\Delta t}f\right\}\\&+\left[G_{Ltrl}\right]\left\{{}_{t+\Delta t}u^{f}\right\}+\left(\left[C_{Ltrl}\right]+\left[G_{CLtrl}\right]\right)\left\{{}_{t+\Delta t}\dot{u}^{f}\right\}\end{aligned} \tag{2.15a}$$

where $\left[H_{0}\right]=\left[\begin{array}{ccc:c:c}I & & O & O & O\\ & \ddots & & \vdots & \vdots\\ O & & I & O & O\\ \hdashline O & \cdots & O & I & \begin{matrix}O\\ H\end{matrix}\\ \hdashline O & \cdots & O & O & I\end{array}\right]$, $\left[R_{0}\right]=\left[\begin{array}{ccc:c:c}I & & O & O & O\\ & \ddots & & \vdots & \vdots\\ O & & I & O & O\\ \hdashline O & \cdots & O & \begin{matrix}I & O\\ O & R\end{matrix} & O\\ \hdashline O & \cdots & O & O & I\end{array}\right]$ (2.15b, c)

Here H is a kind of connection matrix for force equilibrium between rigid foundation and superstructure. When restoring force of superstructure $\{p^s\}$ has one DOF in lateral x-coordinate, which satisfies the equilibrium shown in Fig. 2.3(a). There is a relationship between $\{p^s\}$ and the restoring force on the representative nodes $\{\hat{p}_R^g\} = \{p_x \quad p_z \quad m_{zx}\}^T$ with H in RHS of Eqn. 2.15b, as shown below.

$$\{\hat{p}_R^g\} = H\{p^s\} \text{ where } H = \begin{bmatrix} -1 & 0 & h \end{bmatrix}^T \tag{2.16a}$$

Whereas displacement of structure $\{u^s\}$ and the representative node of rigid foundation $\{\hat{u}_R^g\} = \{u_x \quad u_z \quad \theta\}^T$ shown in Fig. 2.3(b) satisfies the equation below.

$$\{u^s\} = H^T\{\hat{u}_R^g\} \tag{2.16b}$$

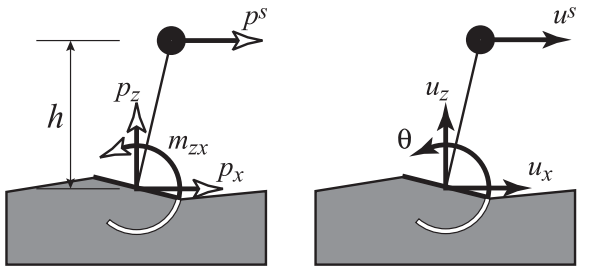

(a) Force equilibrium (b) Displacement continuity

Figure 2.3. Relationships in force and displacement of superstructure and foundation

The coefficient matrices [M], [C], and [K] in Eqns. 2.3, 2.4, and 2.15 are given as follows.

$$[M] = [R_0][M_0][R_0^T] \tag{2.17}$$
$$[C] = [H_0][R_0][C_0][R_0^T][H_0^T] \tag{2.18}$$
$$[K] = [H_0][R_0][K_0][R_0^T][H_0^T] \tag{2.19}$$

where

$$[M_0] = \left[\begin{array}{ccc|c} \left[M_{FF}^g\right]_{II}^{(1)} & & O & \left[M_{FF}^g \quad M_{FR}^g\right]_{IB}^{(1)} N_B^{(1)T} & O \\ & \ddots & & \vdots & \vdots \\ O & & \left[M_{FF}^g\right]_{II}^{(n)} & \left[M_{FF}^g \quad M_{FR}^g\right]_{IB}^{(n)} N_B^{(n)T} & O \\ \hline N_B^{(1)}\begin{bmatrix} M_{FF}^g \\ M_{RF}^g \end{bmatrix}_{BI}^{(1)} & \cdots & N_B^{(n)}\begin{bmatrix} M_{FF}^g \\ M_{RF}^g \end{bmatrix}_{BI}^{(n)} & \sum_{k=1}^{n} N_B^{(k)}\begin{bmatrix} M_{FF}^g & M_{FR}^g \\ M_{RF}^g & M_{RR}^g \end{bmatrix}_{BB}^{(k)} N_B^{(k)T} & O \\ \hline O & \cdots & O & O & M^s \end{array}\right] \tag{2.20}$$

$$[C_0] = \left[\begin{array}{ccc|c} \left[C_{FF}^g\right]_{II}^{(1)} & & O & \left[C_{FF}^g \quad C_{FR}^g\right]_{IB}^{(1)} N_B^{(1)T} & O \\ & \ddots & & \vdots & \vdots \\ O & & \left[C_{FF}^g\right]_{II}^{(n)} & \left[C_{FF}^g \quad C_{FR}^g\right]_{IB}^{(n)} N_B^{(n)T} & O \\ \hline N_B^{(1)}\begin{bmatrix} C_{FF}^g \\ C_{RF}^g \end{bmatrix}_{BI}^{(1)} & \cdots & N_B^{(n)}\begin{bmatrix} C_{FF}^g \\ C_{RF}^g \end{bmatrix}_{BI}^{(n)} & \sum_{k=1}^{n} N_B^{(k)}\begin{bmatrix} C_{FF}^g + C_{Btm}^g + C_{LRFB}^g & C_{FR}^g \\ C_{RF}^g & C_{RR}^g \end{bmatrix}_{BB}^{(k)} N_B^{(k)T} & O \\ \hline O & \cdots & O & O & C^s \end{array}\right] \tag{2.21}$$

$$[K_0] = \left[\begin{array}{ccc|c} \left[K_{FF}^g\right]_{II}^{(1)} & & O & \left[K_{FF}^g \quad K_{FR}^g\right]_{IB}^{(1)} N_B^{(1)T} & O \\ & \ddots & & \vdots & \vdots \\ O & & \left[K_{FF}^g\right]_{II}^{(n)} & \left[K_{FF}^g \quad K_{FR}^g\right]_{IB}^{(n)} N_B^{(n)T} & O \\ \hline N_B^{(1)}\begin{bmatrix} K_{FF}^g \\ K_{RF}^g \end{bmatrix}_{BI}^{(1)} & \cdots & N_B^{(n)}\begin{bmatrix} K_{FF}^g \\ K_{RF}^g \end{bmatrix}_{BI}^{(n)} & \sum_{k=1}^{n} N_B^{(k)}\begin{bmatrix} K_{FF}^g & K_{FR}^g \\ K_{RF}^g & K_{RR}^g \end{bmatrix}_{BB}^{(k)} N_B^{(k)T} & O \\ \hline O & \cdots & O & O & K^s \end{array}\right] \tag{2.22}$$

Substituting from Eqn. 2.17 to Eqn. 2.19 into Eqns. 2.3, 2.4, and 2.15, the effective stiffness matrix, the effective nodal force vector, and the unbalanced force vector are obtained. These vectors and matrices have to be given separately as DOF of internal nodes, total boundary nodes, and structure nodes. In parallel computing, each processing node has only to make and memorize required vectors and matrices for the node. The flowchart is shown in Fig. 2.4. White-on-black items in this chart are parallelized processes.

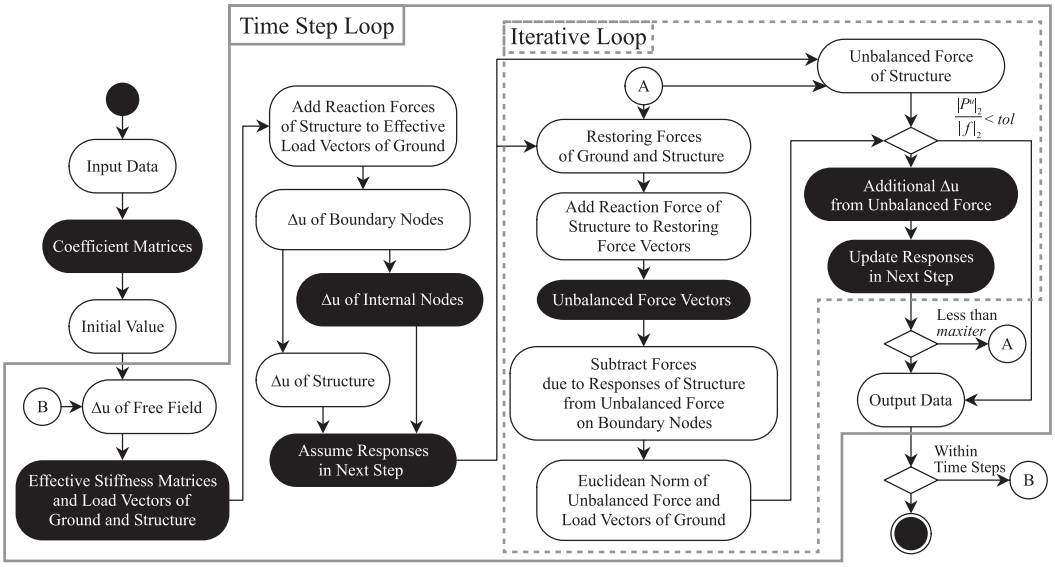

Figure 2.4. Program flowchart

3. FREE VIBRATION ANALYSIS OF A STRUCTURE ON ELASTIC GROUND

To analyze performance and to verify results, free vibration analysis of ground model with a superstructure shown in Fig. 3.1 was executed.

3.1. Analytical Model

Ground was modeled with 8-node hexahedral isoparametric elastic elements. On the lateral and bottom ground boundary there were three-dimensional viscous boundary, except that the vertical DOFs on bottom boundary were fixed. Soil density was 1.7 t/m^3, Poisson ratio was 0.35, and intrinsic attenuation was 0 %. There were two cases of shear wave velocity: 150 and 300 m/s. A part of ground in the model was transformed to rigid spread foundation, on which single-degree-of-freedom superstructure was. The foundation was a square 20 m on each side without thickness.

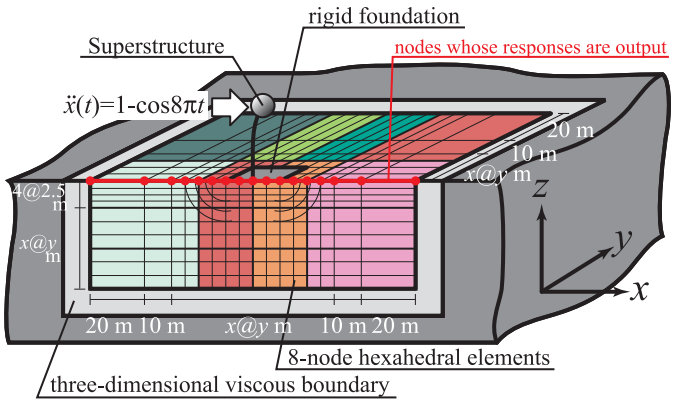

Figure 3.1. Analytical model

Size of ground in depth direction was 50 m, and there were three cases for horizontal directions: 100 m, 200 m, and 400 m (Table 3.1). In addition, there were three cases for size of elements (variant *y* in Figure 3.1): 10 m, 5 m, and 2.5 m.

Table 3.1. Size of ground

Case	x-direction	y-direction	z-direction
g100	100 m	100 m	50 m
g200	200 m	200 m	
g400	400 m	400 m	

The superstructure was modeled by undamped elastic single-degree-of-freedom shear spring model. Each story was a square 20 m on each side, and its weight *m* was 480 t. There were four cases of number of stories *n*: 3, 6, 9, and 12. The story height *h* was 3.33 m. The elastic natural period T_S considering fixed-base are calculated by $0.02nh$ s. To reduce the DOFs of structure to one DOF, an *n*-DOF model was made at first, and inverted-triangle-shaped first eigenmode was assumed to the *n*-DOF model. Therefore, equivalent mass $\overline{M}$ and equivalent height $\overline{H}$ were calculated by Eqn. 3.1, and equivalent stiffness was calculated from $\overline{H}$ and T_S.

$$\overline{M} = \frac{\left(\sum_{i=1}^{n} m \cdot {}_1u_i\right)^2}{\sum_{i=1}^{n} m \cdot {}_1u_i^2} = \frac{3n(n+1)}{2(2n+1)}m, \quad \overline{H} = \frac{\sum_{i=1}^{n} m \cdot {}_1u_i \cdot H_i}{\sum_{i=1}^{n} m \cdot {}_1u_i} = \frac{1}{3}(2n+1)h \tag{3.1a, b}$$

where ${}_1u_s$ is the first eigenvector of the *i*-th story, and H_i is the height from ground level to the *i*-th story.

4. ANALYTICAL RESULTS OF FREE VIBRATION

For free vibration analysis, a cycle of acceleration $\ddot{x}(t) = 1 - \cos 8\pi t$ m/s^2 was input only to the node of superstructure, in which *t* is elapsed time. Analysis time was 4.0 s and time interval for integration was 0.01 s.

4.1. Processing Time for Calculation

Out of total 9 cases by ground size (g100, g200 and g400) and element size (e10, e5 and e2.5), cases except for g400+e2.5 were processed on HA8000 cluster system in Information Technology Center, The University of Tokyo. The number of elements and DDM partitions in three directions, the number of DOFs, and the number of processing nodes are shown in Table 4.1. However, because the size of case g400+e2.5 was too large to be calculated in time limit of personal course of HA8000 cluster system, it was calculated on another symmetric multiprocessing computer.

Table 4.1. Partitioning for domain decomposition method and degrees of freedom

Case	Elements			Partitions			Degrees of freedom		Number of processes
	x	y	z	x	y	z	Internal nodes on each subdomain, maximum	Total boundary nodes	
g100+e10	8	8	8	2	2	1	675	1431	4
g100+e5	12	12	12	2	2	2	1029	3591	8
g100+e2.5	20	20	20	4	4	2	1188	13959	32
g200+e10	18	18	8	4	4	1	972	5631	16
g200+e5	32	32	12	8	4	2	945	22311	64
g200+e2.5	60	60	20	8	8	4	1458	104631	256
g400+e10	38	38	8	8	8	1	972	22167	64
g400+e5	72	72	12	16	8	2	1260	100311	256
g400+e2.5	140	140	20	16	16	1	6300	376071	16 (on another SMP)

By the method used in this program, the smaller the number of DOFs of internal nodes in each subdomain is, the shorter the processing time can be, but at the same time, because the number of total boundary nodes gets increased, the processing time for total boundary nodes can be longer. Therefore, it is necessary to consider the trade-off determining the best number of partitioning, but in this paper, the number of DOFs of internal nodes was set around 1000 to examine the relationship between the DOFs of total boundary nodes and processing time, as shown in Fig. 4.1 (except for g400+e2.5). It was recognized that the processing time was basically in proportion to the DOFs of total boundary nodes by the analysis.

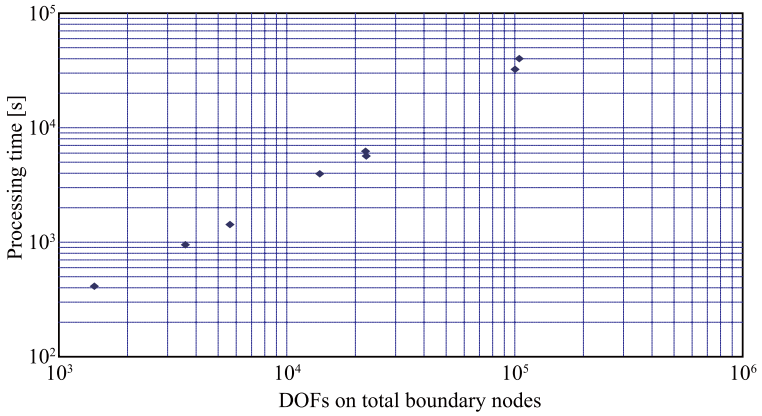

Figure 4.1. Relationship between degrees of freedom of total boundary nodes and average processing time

4.2. Response of Ground and Superstructure

It is vertical response displacement of ground surface (red closed circles in Fig. 3.1) of the case g200+e2.5, V_S=150 m/s, and 3-story building that is shown in Fig. 4.2. It is observed that waves are slightly reflected from lateral boundary. Cases g100, g200, and g400 of case e2.5 and V_S=150 m/s are compared in Fig. 4.3. There is bare difference between g200 and g400, and in the 3-story graphs, there is an conspicuous influence of reflected waves. Cases e10, e5, and e2.5 of case g400 and V_S=150 m/s are compared in Fig. 4.4. When the size of elements are smaller, the period of structure response is longer and the horizontal displacement and rotational angle are higher. When the absolute value of responses are important, it is necessary to make the size of elements smaller than case e2.5.

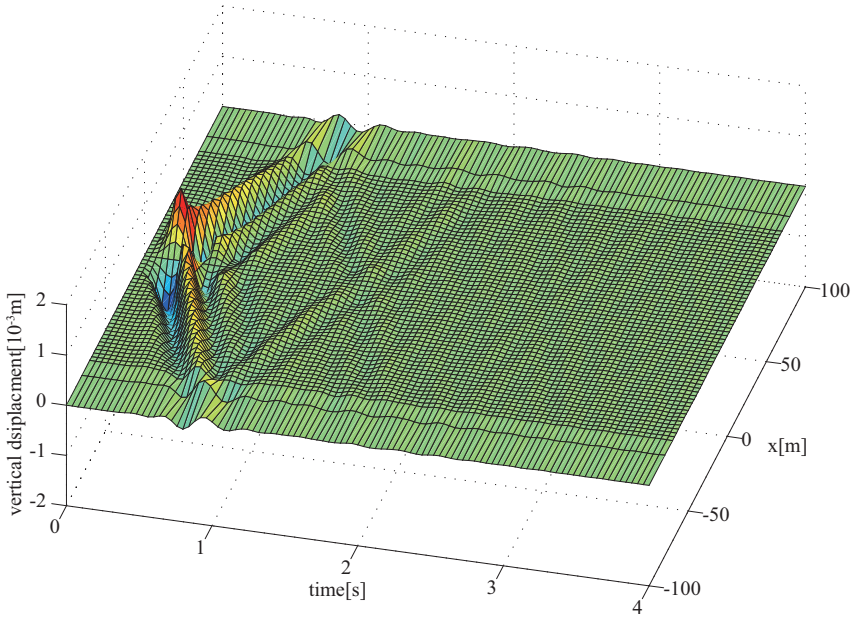

Figure 4.2. Vertical response displacement on surface of ground (g200+e2.5, V_S=150m/s, 3-story)

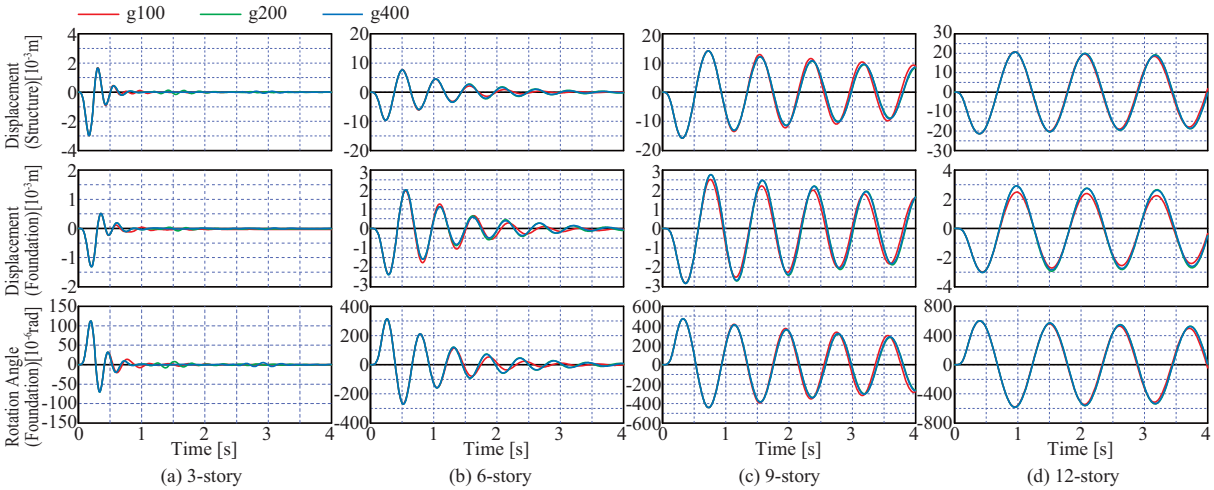

Figure 4.3. Response displacement of superstructure and foundation (Case e2.5, V_S=150 m/s)

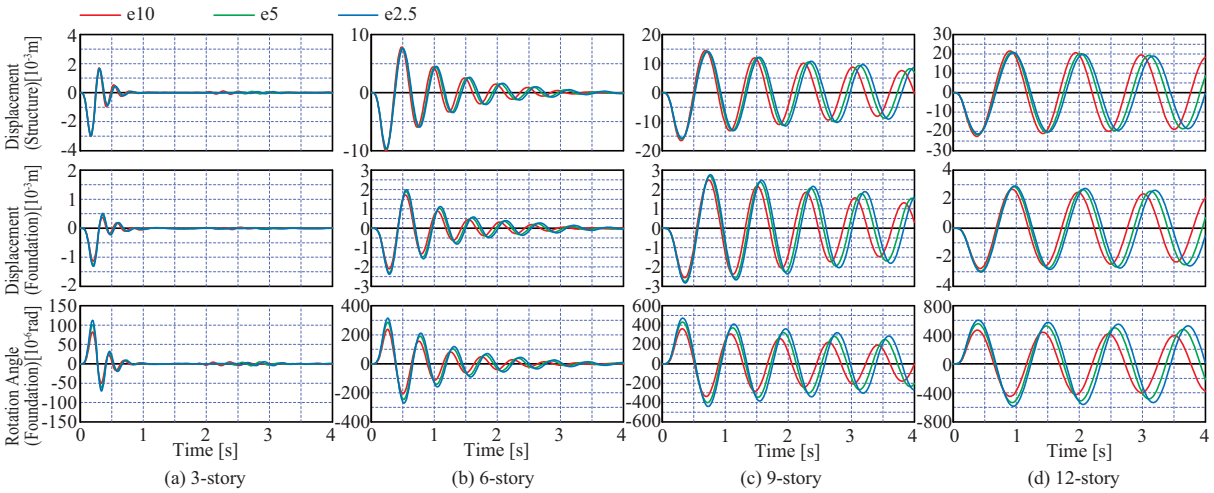

Figure 4.4. Response displacement of superstructure and foundation (Case g400, V_S=150 m/s)

4.3. Equivalent Damping Ratio

To evaluate equivalent damping ratio due to dissipation damping, three cycles of response after the first peak was used by Eqn. 4.1, which is based on amplitude reduction factor.

$$h_i = \frac{1}{2\pi} \log \frac{{}^{t_i}u}{{}_{t_i+T}u} \tag{4.1}$$

where ${}^{t_i}u$ is a peak displacement of structure at t_i s, and T is a period of structure response.

The damping ratios are shown in Fig. 4.5 comparing with values based on the elastic theory (Tajimi, 1959). Fig. 4.5(a) compares the values in different ground sizes of case e2.5. When V_S=150 m/s, the value of g200 and g400 were almost the same value, but that of g100 differed from them approximately from -0.6% to +1.5%. Fig. 4.5(b) compares the values in different element sizes of case g400. When V_S=150 m/s, the value of e5 and e2.5 were almost the same value, but that of e10 differed from them approximately from -1.9% to +0.8%. In the cases of V_S=300 m/s, the differences of the values were smaller than the cases of V_S=150 m/s. In addition, comparing with the values based on the elastic theory in Fig. 4.5, the values by FEM analysis were between lines of sway-only case and rocking-only case.

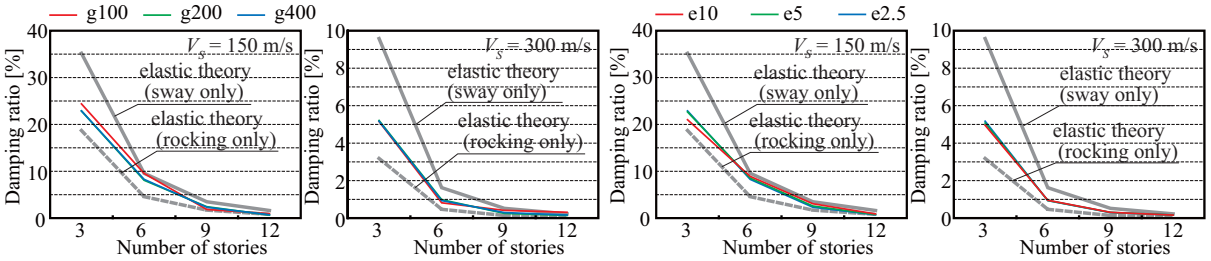

(a) Case g100, g200 and g400 of e2.5 (b) Case e10, e5 and e2.5 of g400

Figure 4.5. Damping ratios comparing with values by elastic theory

5. SUMMARY AND CONCLUSIONS

In this paper, a parallelizing method for soil-structure dynamic response analysis is described, and through free vibration analysis, conclusions listed below are obtained.

1) Through the analysis on HA8000 cluster system, it was recognized that the required processing time was basically in proportion to the degrees of freedom of problems that have less than a few hundred thousand degrees of freedom.

2) To reduce the influence of reflected waves when the structure is on the soft ground (Vs = 150 m/s), it was necessary that horizontal size of ground was more than 20 times larger than the size of foundation. In addition, when the absolute values of responses are important, size of ground element around foundation need to be less than 2.5m on each side.

3) In comparison with theoretical values of damping ratio due to dissipation damping based on the elastic wave theory, the damping ratio calculated from amplitude reduction factors of response is between the theoretical values of sway-only case and rocking-only case. In the case e2.5 of V_S=150 m/s, the value of g200 and g400 were almost the same value, but that of g100 differed from them approximately from -0.6% to +1.5%. In the case g400 of V_S=150, the value of e5 and e2.5 were almost the same value, but that of e10 differed from them approximately from -1.9% to +0.8%.

ACKNOWLEDGEMENT

The analysis in this paper was processed on HA8000 cluster system in Super Computing Division, Information Technology Center, The University of Tokyo.

REFERENCES

Tajimi, H. (1959). Basic theories on aseismic design of structures, *Report of the Institute of Industrial Science, the University of Tokyo*, **8:4**, 170-215

Barrett, R., Berry, M., Chan, T.F., Demmel, J., Donato, J.M., Dongarra, J., Eijkhout, V., Pozo, R., Romine, C., and Van der Vors, H. (1994). Templates for the Solution of Linear Systems: Building Blocks for Iterative Methods, SIAM

Soneda, N., Yagawa, G. and Yoshimura, S. (1991). Elastic-plastic finite element analysis using domain decomposition method, *11st International Conference on Structural Mechanics in Reactor Technology*, **B:** 243-248